Interpretation of stress variation in silicon nitride films deposited by electron cyclotron resonance plasma

Marie-Paule Besland, Mickael Lapeyrade, Franck Delmotte, Guy Hollinger

Interpretation of stress variation in silicon nitride films deposited by electron cyclotron resonance plasma

M. P. Besland[a)] and M. Lapeyrade
LEOM, UMR CNRS 5512, Ecole Centrale de Lyon, BP 163, 69131, Ecully, Cedex, France

F. Delmotte
Laboratoire Charles Fabry de l'institut d'Optique, Université Paris XI, BP 147, 91403, Orsay, France

G. Hollinger
LEOM - UMR CNRS 5512, Ecole Centrale de Lyon, BP 163, 69131, Ecully, Cedex, France

We report here on internal stress variations in SiN_x films deposited on silicon by plasma enhanced chemical vapor deposition-electron cyclotron resonance (PECVD-ECR) plasma. The effects of deposition parameters, film thickness and surface morphology have been considered. SiN_x films can exhibit a compressive or a tensile internal stress, ranging from −1970 to +465 MPa, depending on deposition parameters. Among published results, usual reported residual stress for PECVD films is compressive. Versatility of our experimental ECR equipment allows one to deposit films exhibiting a weak stress in the range of a few tens MPa. On the basis of atomic force microscopy observations, a correlation between the intensity of the stress and the granular morphology of the films has been observed. The rms value for SiN_x film surfaces is never higher than 1.5 nm, with a grain height ranging from 1.2 to 5 nm and a grain width varying from 20 to 60 nm. Both the grain size and the residual stress vary with the thickness of the films. This work highlights the influence of the initial surface properties on the deposition mechanism. An exhaustive review of the stress generation model is given and a tentative interpretation for the origin of stress, either compressive or tensile, is proposed. © *2004 American Vacuum Society.* [DOI: 10.1116/1.1776179]

I. INTRODUCTION

Si_3N_4 dielectric films are widely used for microelectronics, optoelectronics and microelectromechanical system (MEMS) devices. This includes passivation, masks for lithography or ion implantation, optical coatings or waveguides and films for MEMS. Deposition techniques, involving low energy species, such as electron cyclotron resonance-plasma enhanced chemical vapor deposition (ECR-PECVD)[1,2] and distributed electron cyclotron resonance (DECR)[3] techniques, have been developed recently to produce, at low temperature, high quality dielectric SiN_x films. It was found that, as for conventional rf PECVD techniques, the films generally exhibit a residual stress, which could be dependent, as mentioned earlier in the literature,[4,5] on the deposition technique and parameters. Over the past years, a large amount of stress data has been reported for films prepared in various conditions. General trends emerge from the numerous publications dedicated to the subject. It appears that films deposited by techniques involving high energy and physical mechanisms, like reactive ion sputtering[6,7] and high rf bias,[8,9] lead to highly compressive strained films. PECVD techniques, involving low rf bias at relatively low temperature (≤400°C), allow the stress to be reduced at lower compressive values.[10] However, CVD deposition techniques, performed in a high temperature range (typically 650–850°C), induce tensile strain in the films,[11] mainly correlated to high density.[12] Works also report the possibility of obtaining both types of film, i.e., compressively or tensely strained films, with the same technique, by varying deposition parameters, like deposition pressure,[13] gas phase composition,[14,15] addition of an inert gas[16] or bias variation.[17] The use of a hydrogenated gas in the plasma can also favor the decrease of internal stress.[18] Some workers have succeeded in defining experimental conditions for low stress film deposition.[8,19,20]

At the same time, a large number of studies have been dedicated to the understanding of this internal stress generation.[21–23] Most publications have reported the participation of two contributions for the residual stress in thin films reported on a substrate, namely a thermal and an intrinsic contribution. To a large extent, the approach of Cammarata[24] appears as the most relevant. Indeed, the residual stress can be expressed by the sum of three contributions: (i) thermal stress due to differences in the thermal expansion coefficients of the film and substrate, (ii) epitaxial or coherency stress due to lattice matching between film and substrate, (iii) intrinsic stress which refers to the stress produced by a change of film density during or after deposition. When compared to crystalline film epitaxy, the amorphous film growth process like the plasma growth process is not well understood. A granular morphology in evaporated films can arise from limited surface diffusion and competition

---
[a)]Author to whom correspondence should be addressed. Present address: Laboratoire des Plasmas et des Couches Minces, Institut des Matériaux Jean Rouxel, UMR CNRS 6502, Université de Nantes, BP 32229, 44322 Nantes, Cedex 3, France; electronic mail: marie-paule.besland@cnrs-imn.fr

shadowing in a so-called "columnar" growth,[25] early observed for sputter-deposited thin films.[26] Nucleation can be favored when the surface free energy of a deposited film plus the free energy of the film-substrate interface is higher than the free energy of the substrate surface.

Even if the microscopic origin of intrinsic stress in the films is recurrently a matter of discussion,[27–30] and despite an increasing technological interest, few reports are dedicated to the study of residual stress in ECR films.[22,27,31]

First of all, in order to achieve an actual stress reduction in SiN$_x$ films deposited by ECR plasma on silicon substrates, we have studied a large range of process parameters: deposition temperature, ranging from room temperature to 300 °C, and deposition pressure in the 0.65–2.4 mTorr range. As a result, we have specified experimental conditions to achieve such a stress reduction. As we did so, we have obtained some insights into the stress process itself by studying: (i) the stress distribution between substrate and film as the film thickness increases, (ii) the initial roughness of the substrate as an important factor for the film/substrate coherence, and (iii) the surface film morphology as a fingerprint of the intrinsic film texture.

II. EXPERIMENT

SiN$_x$ film depositions were carried out in a plasma reactor, which is part of an ultrahigh vacuum x-ray photoelectron spectroscopy (XPS) multi-chamber system, including an XPS surface analysis chamber. The plasma is produced by an Astex ECR S-250 compact source, with low microwave power (2.45 GHz), tunable up to 250 W. The precursor gases are N$_2$, which is introduced in the plasma source and SiH$_4$, which is injected through a dispersal ring. On the basis of previous optimization of the process,[32] the deposition parameters were chosen as follows: microwave power 200 W, electromagnetic coil supply current 22 A, substrate to source distance 22 cm.

Substrates used in. this work were *p*-type (100) oriented 2 in silicon wafers from ACM, whose thickness is in the 380 μm range. Film thickness, ranging from 400 to 2000 Å, refractive index and homogeneity were checked *in situ* by ellipsometric measurements, performed at an incidence angle of 70.5°, with a commercial phase modulated ellipsometer (Jobin-Yvon UVISEL) mounted on the plasma chamber through viewports equipped with strain free fused quartz windows.

In situ ellipsometric measurements, calibrated to a pyrometer and the melting points of In and InSb, were used for a precise surface temperature control. The sample was heated using a manually controlled filament which permits heating up to 600 °C. To calibrate the variation of the ellipsometric parameters, Ψ and Δ, with the temperature, we added two pieces of indium and of InSb on the sample holder close to the substrate, which enabled use of the reference of the room temperature (20 °C) and the melting points of indium (156 °C) and InSb(525 °C). Above 250 °C, a pyrometer was used to correlate ellipsometric measurements to temperature. Details on temperature calibration procedure have been pub-

lished earlier by co-workers.[33,34] This procedure allows a very accurate control of the surface temperature, at each step of the process.

The chemical composition of the films was determined both by *in situ* x-ray XPS surface analysis and *ex situ* nuclear reaction analysis. Atomic force microscopy (AFM) observations were performed *ex situ* to study the surface morphology of the films. Each series of films was observed with the same tip and lateral dimensions given after a reductive correction of 30%–40% to take into account the enlargement of grains size by the tip.

The etch rate is known to be very sensitive to the density of the film and to its hydrogen content.[37–39] The etch rate was measured in a dilute solution (1:7) of commercial buffered oxide etchant (NH$_4$F/HF/H$_2$O:40/49/11) in de-ionized water. In the same conditions, a low pressure chemical vapor deposition (LPCVD) silicon nitride, used as a reference, was characterized by an average etch rate of 4 Å min^{-1}. At least, the half thickness of the films was etched to check their homogeneity in depth.

We studied the variation of the mechanical properties of the films versus: (i) the film thickness; (ii) the substrate temperature [room temperature (RT) to 300 °C]; and (iii) the total pressure, in the range of 0.65–2.4 m Torr, at fixed gas flow rate ratio N$_2$/SiH$_4$=15.

The stress in our films has been calculated by the bend-bending method, where the radius of the bent, coated substrate is determined and used to calculate the residual stress. Recently Freund[35] and co-workers extended the use of the simplified form of Stoney's formula[36] to a broader class of film-substrate configurations. In our case, we can properly assume that geometrical requirements and mechanical assumptions[37] are verified: (i) the film and the substrate thickness are small compared to the lateral dimensions, (ii) the substrate thickness is much greater than the film thickness, (iii) the film thickness is uniform with good adhesion to the substrate, (iv) the stress is isotropic, without any preferential direction, i.e., the curvature of the substrate is uniform, (v) the deformation both for the film and the substrate is situated in the elastic domain. The internal stress in the deposited film is calculated from the change in the substrate curvature from $\tau_0=1/R_0$ for the bare substrate to $\tau=1/R$ after the thin film deposition, with the following formula:

$$\sigma = \frac{E_s \cdot t_s^2}{6(1 - \nu_s) \cdot t_f} \cdot \left(\frac{1}{R} - \frac{1}{R_0} \right),$$

where R_0 is the radius of curvature of the bare Si substrate and R is the radius of curvature after the deposition of the film on the substrate, E_s and ν_s are, respectively, the Young's modulus and Poisson ratio of the substrate, and t_s and t_f are the thickness of the substrate and the film, respectively, equal to 380 μm and in the 800–1000 Å range. The value of $E_s/(1-\nu_s)$ for substrate Si(100) is 1.8×10^{11} Pa. The accuracy of the stress value varies in the +/−30–80 MPa range. The variation of substrate curvature has been checked by interferometry. The estimation is based on the analysis of Newton's rings which appear after reflection of a monochro-

TABLE I. Deposition parameters and characteristics for SiN$_x$ films of this study. For all films the other experimental parameters were as follows: Microwave power of 200 W, electromagnetic coil current supply 22 A, source to substrate distance of 22 cm, gas flow rate ratio N$_2$/SiH$_4$=15.* The hydrogen content is given in % of atoms/cm^2.

Sample	Radius R_0 (m)	Radius R_1 (m)	T_S (°C)	Pressure (mTorr)	Thickness (Å)	Deposition rate (Å/min)	Optical index at 3 eV	N/Si ratio (XPS)	%H content*	Density g cm^{-3}	Etch rate (Å/min)[a]	Stress (MPa)[b]
S120			RT	1.2	800	13	1.96	1.45	14	2.77	300	−554
S122			200	1.2	810	9	2.02	1.4	9	2.87	80	−452
S124			300	1.2	750	8	2.06	1.33	6	3.04	10	−704
S170	~0	−96	200	1.2	430	9.6	2	⋯	⋯	⋯	⋯	625
S160	−139	−39	200	1.2	820	9.5	2	1.33	⋯	⋯	85	−600
S165	−127.5	−45.6	200	1.2	795	9	2	1.4	⋯	⋯	90	−480
S171	358	−46.8	200	1.2	1500	10	1.99	⋯	⋯	⋯	⋯	−446
S172	1075	−29	200	1.2	2090	10	2	⋯	⋯	⋯	⋯	−460
S174			200	0.65	740	9	2	1.51	10	2.83	380	−1970
S175			200	1.75	720	7	1.96	1.4	⋯	⋯	150	+356
S163	−139	182	200	2	830	7	1.95	⋯	⋯	⋯	⋯	+410
S164	−336	248	200	2.33	870	7	1.96	1.41	8	2.85	520	+220
S127			200	2.4	890	7.5	1.95	⋯	9	⋯	⋯	+465

[a]Etching solution: BOE:H$_2$O=1:7.
[b]Convention: += concave and −= convex.

matic light (namely λ=535 nm of a thallium lamp) on the substrate through an optically flat quartz window.[7]

III. RESULTS

A. Internal stress measurements

Our measurements were analyzed through a raw application of Stoney's formula using the data curvature changes presented in Table I.

In standard deposition conditions, i.e., P_w=200 W, I_B=22 A, D=22 cm, T_{sub}=200 °C, and total pressure of 1.2 mTorr, the 800 Å ECR SiN$_x$ films exhibit a compressive internal stress in the range of −580 to −450 MPa, giving a mean value of −520+/−60 MPa. This observation is the most common behavior for dielectric films deposited by plasma enhanced techniques.[4,9,31,38] We measured the evolution of the internal stress for films deposited in standard conditions, i.e., 1.2 mTorr and 200 °C, with increasing thickness, in the 400–2000 Å range (Fig. 1). As the thickness increases, the total stress first decreases and secondly saturates for a thickness of 1200 Å. Thinner SiN$_x$ films exhibit a higher compressive stress than the thicker films. The same
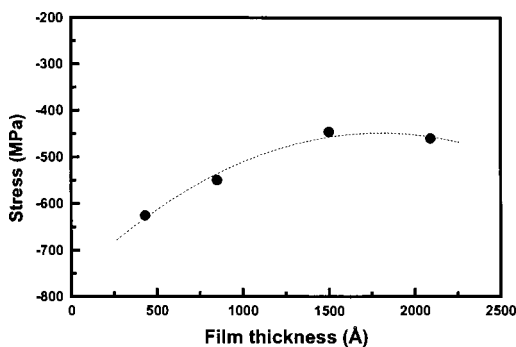
800-Å-thick SiN$_x$ film has been deposited on two silicon substrates, with significant difference in initial roughness (rms of 0.1 and 1.5 nm). The stress values after deposition were, respectively, −580 and −310 MPa. This observation clearly highlights the influence of the substrate morphology on the internal structure of the film.

The effect of the total pressure on the internal stress was investigated for 1000-Å thick SiN$_x$ films. The variation is shown in Fig. 2: as the pressure increases from 0.65 to 2.4 mTorr, the total internal stress varies from a highly compressive (−1970 MPa) to a moderate tensile value (+465 MPa).

The effect of the deposition temperature on the internal stress is shown in Fig. 3. In standard deposition conditions, SiN$_x$ films, obtained with nonintentional heating of the sample, exhibit a compressive strain of −550 MPa and −310 MPa, respectively, for samples S161 and S162. An increase of the deposition temperature to 200 °C promotes a slight variation of the internal stress. A further increase up to 300 °C leads to a higher compressively strained film, at −704 MPa.
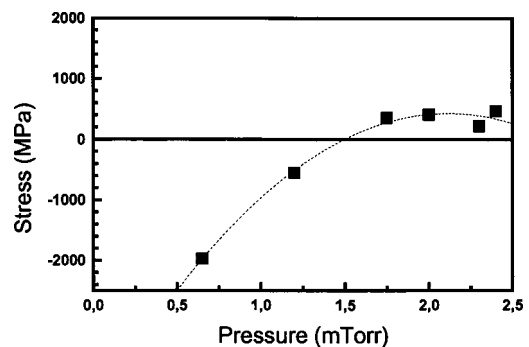

FIG. 1. Variation of the stress vs the thickness of the SiN$_x$ films.

FIG. 2. Effect of the total pressure on the internal stress in the SiN$_x$ films.
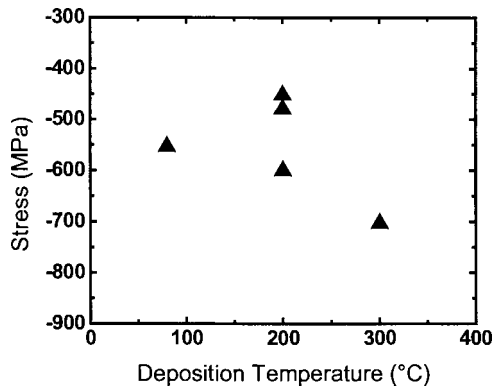
FIG. 3. Variation of the internal stress in SiN$_x$ films vs the deposition temperature.

The thermal stress contribution σ_{th} to the internal stress results from the difference in the thermal expansion of the film and the substrate between the deposition temperature T_d and the measurement temperature T_m, which is RT in that study. σ_{th} can be easily estimated using the following formula:

$$\sigma_{th} = \frac{E_f}{(1 - \nu_f)} \cdot (\alpha_f - \alpha_s)(T_d - T_m),$$

where α_f and α_s are the thermal expansion coefficients for, respectively, the film and the substrate, and equal to 1.55×10^{-6} and 3.2×10^{-6} °C^{-1}, respectively. As the Young's modulus value for the film, the one given for LPCVD SiN$_x$ film[36] has been taken: $E_f / 1 - \nu_f = 3.7 \times 10^{11}$ Pa. Thus, in our experimental conditions and for a deposition temperature ranging from RT to 300 °C, the thermal contribution to the internal stress is -30 and -110 MPa, respectively, and these values are certainly overestimated ones.

In the bottom part of Table II, stress measurements are given for three SiN$_x$ films, with thicknesses in the 700–800 Å range. They were deposited in standard condi-

tions of temperature (200 °C), microwave power and coil supply, (200 W and 22 A, respectively), for a total pressure of 1.75 mTorr and a flow rate ratio N$_2$/SiH$_4$ = 15. The differences between these samples stand in the way of pressure regulation.

For sample S175, the increase of pressure, from the standard pressure (1.2 mTorr) to 1.75 mTorr, was obtained by increasing the flow rate of both nitrogen and silane, from 18.75/1.25 up to 30/2, keeping the total flow rate ratio constant at 15. The film exhibits a tensile residual stress of +356 MPa. In the case of S177, the initial gas inlet is the same as for standard deposition at 1.2 mTorr (Sample S160-S162-S165), but the pumping speed was decreased by closing the pumping valve, resulting in an increase of the deposition pressure up to 1.75 mTorr. The measured stress is very close to no stress (+35 MPa). In the case of sample S176, the deposition pressure was increased to 1.75 mTorr by adding 9 sccm of hydrogen in the gas plasma, resulting in an inlet quantity of nitrogen species equivalent to that of sample S177. The residual stress is compressive at -200 MPa.

The last sample described in Table II (S166) was deposited in standard conditions, except for the coil supply, which was fixed at a lower value of 18 A. The residual stress is once again modified to lower compressive stress, with a value of -300 MPa. The results presented in Table II will be further discussed.

B. AFM observations

AFM observations of 1000-Å-thick films deposited at RT and 200 °C show, in both cases, a granular morphology (Fig. 4) with an average surface roughness of 1.1 and 1.4 nm and a grain lateral dimension of 50 and 20 nm, respectively.

Figure 5 shows the surface morphology of SiN$_x$ films deposited at increasing pressure. It is clearly observed that the grain size is also dependent on the deposition pressure: at low deposition pressure (0.65 mTorr), SiN$_x$ films exhibit

TABLE II. Variation of experimental parameters around the standard conditions of deposition and effects on some properties of the SiN$_x$ films.

Sample[a]	Radius R_0 (m)	Radius R_1 (m)	Pressure (mTorr)	Thickness (Å)	Vd (Å/min)	Optical index at 3 eV	N/SI ratio (XPS)	Etch rate (Å/min)[f]	Stress (MPa)
S161	−225.6	−66.4	1.2	935	11	1.89	/	/	−310
S162	−196	−47	1.2	790	9	1.98	···	···	−550
S166[b]	169	−393	1.2	795	6.5	1.9	1.49	/	−300
S175[c]			1.75	720	7	1.96	1.4	150	+356
S176[d]			1.75	775	9	1.85	1.4	960	−200
S177[e]			1.75	780	11	1.96	1.33	195	+35

[a]Without specifications, the experimental parameters were as follows: Microwave power 200 W, coil current supply (I_b) 22 A, substrate temperature 200 °C, source-substrate distance 22 cm, flow rate ratio N$_2$/SiH$_4$ = 18.75/1.25.
[b]S166, the electromagnetic coil current supply was lowered to 18 A.
[c]S175, higher flow rate ratio N$_2$/SiH$_4$ = 30/2.
[d]S176, increase of the total pressure by addition of 9 sccm H$_2$.
[e]S177, standing gas inlet N$_2$/SiH$_4$ = 18.75/1.25; the higher pressure was obtained by lowering the pumping speed.
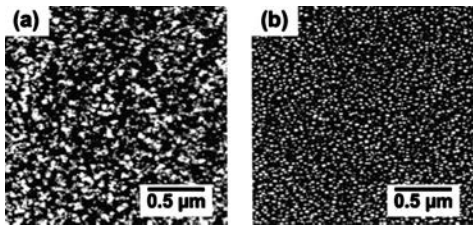[f]Etching solution: BOE:H$_2$O = 1:7.

FIG. 4. AFM images of the SiN$_x$ film surfaces for (a) room temperature deposition and (b) deposition temperature of 200 °C.

TABLE III. Grain size, roughness (deduced from AFM observations) wet etch rate and residual stress of SiN$_x$ film.

Sample[a]	Thickness (Å)	Grain height (nm)	Grain width (nm)	rms (nm)	Etch rate (Å/min)	Stress (MPa)
S120	800	1	50	1.1	300	−554
S174	740	0.8	20	0.2	380	−1970
S165	795	1	20	1.5	90	−480
S127	890	5	60	1.5	500	+465

[a]Experimental deposition parameters are given in Table I.

small grain size and roughness, 0.8 nm (height) and 0.2 nm, respectively. For standard pressure of deposition (1.2 mTorr), both rms and grain height increase, respectively, to 1.5 and 1 nm. For high deposition pressure (2.4 mTorr), the films are made up of larger grains with a height of 5 nm, while the rms remains constant at 1.5 nm.

The typical grain size and roughness of SiN$_x$ films, deduced from AFM observations, are gathered in Table III. It appears that at low pressure, a smooth initial surface and high deposition temperature lead to high compressive stress, correlated to a small grain size (S174). An increase of surface roughness or deposition pressure and a decrease of deposition temperature produce a decrease of the internal stress, associated with an increase of the grain size (S162,S165,S120). Finally, for deposition pressure over 1.5 mTorr, the films are slightly tensely strained and made up of larger grains (S127). For the highest pressure studied, the highest grain size was observed with the same rms of 1.5 nm.

The evolution of the granular morphology during the first stages of deposition was controlled by AFM observations. Typical values are given in Table IV. A granular morphology is observed even for very thin films of 30 Å (sample S190) produced by direct nitridation of silicon [Fig. 6(a)]. The observed rms of 0.1 nm is similar to that of a bare silicon substrate, observed after removal of the native oxide by a HF dip. For a 180-Å-thick SiN$_x$ film (sample S191), deposited on Si in standard conditions at 200 °C [Fig. 6(b)], the rms increases to 0.3 nm, and the grain height grows up from 0.2 to 1 nm, while a similar width of grain of 23–25 nm is observed at the two stages.

As a first observation, these results show a correlation between the intensity of the stress and the granular morphology of the films: as the compressive strain increases, the grain size decreases. It appears that larger strains are observed for smoother surfaces and thinner films.

IV. DISCUSSION

As mentioned in the Introduction, among the various published models for residual stress generation in thin deposited films, the Cammarata's approach[24,39] appears the most relevant to the results of this study. The residual stress is considered as the sum of three contributions: (i) thermal stress due to differences in the thermal expansion coefficients of
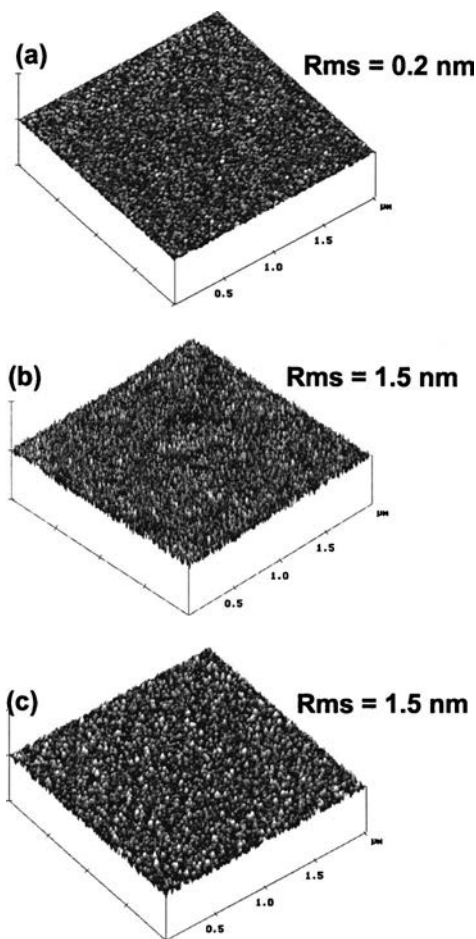

FIG. 5. Typical top-view AFM images of surface morphology vs the deposition pressure: (a) low pressure 0.65 mTorr, (b) standard pressure 1.2 mTorr, and (c) high pressure 2.3 mTorr.

TABLE IV. Grain size and roughness of silicon surfaces and first stages of SiN$_x$ deposition, as deduced from AFM observations.

Sample	rms (nm)	Grain height (nm)	Grain width (nm)	Film Thickness (Å)
S161[a]	0.1	0.1	20	No film
S162[b]	1.5	2–4	30–40	No film
S190[b]	0.1	0.2	23	30
S191[c]	0.3	1	25	180

[a]Experimental deposition parameters are given in Table II.
[b]Sample obtained by direct nitridation of a Si substrate.
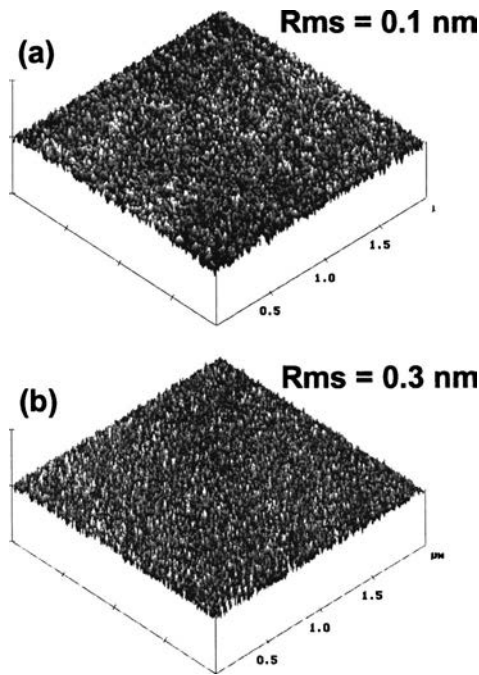[c]Deposited in standard experimental condition of sample S160.

FIG. 6. Top-view AFM images (2 × 2 mm) of the first stages of SiN$_x$ film deposition on silicon substrate (a) 30 Å SiN$_x$ (nitrided Si) and (b) thin 180 Å SiN$_x$ film.

the film and substrate, (ii) epitaxial stress due to lattice matching between film and substrate, (iii) intrinsic stress which refers to the stress produce by a change of film density during or after deposition.

As the thermal stress contribution, in our experimental conditions, is never higher than 100 MPa (as estimated in the previous section), other phenomena must be involved to explain our observations. Our results show that the Si$_3$N$_4$ films have a granular morphology even for very thin films, produced by direct nitridation of silicon (sample S190). Compressive stress is observed in most cases. Figure 1shows that the highest strains are found for the thinnest films. We think that this behavior can be attributed to a planar epitaxial strain associated with a molar volume change in the silicon network at the Si/Si$_3$N$_4$ interface.[40]

As the Si$_3$N$_4$ film is highly compressively strained near the interface, stress relaxation can produce three-dimensional (3D)-island nucleation in addition to surface diffusion.[41] Increasing the thickness of the nitride layer leads to a decrease of the strain associated with some partial relaxation favored by the flexibility of the Si$_3$N$_4$ amorphous network and the 3D morphology. For thicknesses above 1500 Å, the stress is observed to stabilize (Fig. 1). A saturation at the same value has been reported by French and co-workers[20] for LPCVD SiN$_x$ films. This epitaxial strain interpretation is also supported by the fact that rough silicon surfaces lead to lower stressed films rather than smooth surfaces: stress is dependent on the substrate's nature (samples S161, S162).

The results shown in Fig. 2 indicate that intrinsic stress may play a major role in some conditions, since a SiN$_x$ film may exhibit a compressive stress, a tensile stress or no stress

depending only on the pressure in the reactor. Various models[7,12,21–23] have been involved in the literature to explain the origin of tensile and compressive intrinsic stress. A strong correlation exists between this intrinsic stress, the hydrogen content[11] and the density of the films.[18,42]

Silicon nitride films can be deposited either using ammonia NH$_3$ or nitrogen N$_2$ as a precursor. When ammonia is used, SiN$_x$ films exhibit mainly a weak tensile residual stress.[18,43] In this study, considering the physico-chemical characteristics given in Tables I and II, no simple and evident correlation can be highlighted. Since low density, i.e., high etch rate, was observed either for compressive residual stress (samples S174 and S176) or tensile residual stress (samples S164, S175, S177). Likewise, the transition from compressive to tensile residual stress is not correlated either, for our samples, to the chemical composition and the Si concentration in the film,[14,22] since we never obtained N/Si ratios lower than the stoichiometric value 1.33, i.e., Si-rich films.[32] Taylor[10] has shown, through Fourier transform infrared (FTIR) analysis of PECVD SiN$_x$ thin films, a correlation between the intensity of intrinsic compressive stress and the ratio between N–H and Si–H bonds: N–H rich films exhibited highly compressive stress. In that study, the correlation of the stress with the hydrogen content is observed only when the deposition temperature is varied (Fig. 3). Higher residual stress is observed for a higher deposition temperature (samples S120-122-124 in Table I) where the hydrogen concentration is lower (see also Ref. 32). Denser films exhibit low hydrogen content and higher compressive stress.

Some models involve material modification during deposition or structural evolution due to aging with atmospheric moisture.[44,45] The general behavior is a considerable increase in compressive stress, promoted by structural changes in the network by Si–O–Si bridge formation. Such relaxation of stress has also been observed in the case of fluorinated Si–O–F thin films.[27] The evolution of residual stress in our films under aging was not investigated. Nevertheless, this model cannot be invoked to explain the evolution towards tensile residual stress.

In a few words, the various correlations reported in the literature for PECVD thin films are in agreement with our observations for the low pressure range, i.e., lower than 1.2 mTorr. However, the transition to tensile strained films at higher pressure cannot be explained by the previously discussed mechanism.

Nevertheless, this is a well known behavior for thin films deposited by sputtering techniques.[26,46] Typically at low pressure, ion bombardment plays an important part in the deposition mechanism, leading to a tightly packed columnar structure. The deposited films are compressively stressed, due to a great forward sputtering. At higher pressure, however, because of a shorter mean free path and a high number of collisions, the energy of ionic species impinging the surface is weak, promoting a more porous columnar structure. Tensile stress is generated through attractive inter-atomic forces between columns in the porous structure. Thus, while the working pressure increases, a typical compressive-to-
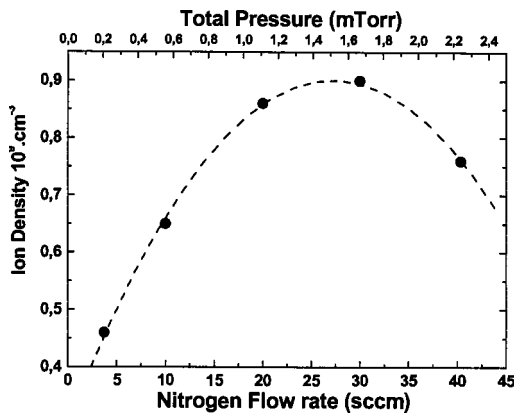
FIG. 7. Variation of ion density vs nitrogen flow rate and total pressure for standard plasma parameters (microwave power 200 W, coil current supply 22 A) measured at sample location, i.e., 22 cm from the source exit.

tensile transition is observed for sputtered films. Intrinsic tensile stresses are created through coalescence of neighboring islands. Similar models for the generation of tensile stress in amorphous thin films have been considered only very recently by researchers.[47,48]

Thus, to understand this particular behavior of our ECR films, two characteristics have to be considered: on the one hand, the ion density versus the deposition pressure (Fig. 7) and, on the other hand, the ion energy (Table V). At low pressure, the ion density is the lowest (0.7×10^9 cm^{-3}) and the ion energy is the highest (32 eV). As a result, the ion bombardment is strong and tends to induce strong compressive stresses in the films. Actually, we measured a high compressive stress of -1970 MPa. As the pressure increases to 1.2 mTorr, the ion density reaches the highest values range, around 0.9×10^9 cm^{-3}. Meanwhile the ion energy decreases to 24 eV, as a consequence of the higher probability of ion collisions. This leads to a decrease of the ion bombardment effect and the generation of a lower compressive stress in the SiN$_x$ films (-500 MPa), in agreement with the literature.[8,9] The further variation of the internal stress with a further increase of the deposition pressure up to 2.3 mTorr is less expected. At high pressure, the ion energy still decreases to 16 eV, whereas the ion density shows a significant decrease down to 0.75×10^9 cm^{-3}. Therefore, the compressive effect due to ion bombardment continues to decrease. Nevertheless,

the origin of the tensile stress measured in such a pressure range cannot be easily understood on the basis of the ion density decrease alone.

To a large extent, the way of varying the deposition pressure in our equipment should be taken into account. Indeed, our plasma chamber is not equipped with a variable pumping speed valve. Thus, the total pressure is directly dependent on the gas flow inlet. This means that, at higher pressure, the amount of species introduced in the chamber is higher. Nevertheless, the ion density measured at the sample location is lower and, in addition, the ion energy is lower, too. We can thus conclude that the concentration of unionized species is higher, with no contribution in the ionic bombardment.

This is indeed supported by the results obtained with samples S175 and S177, deposited at the same total pressure of 1.75 mTorr but with different gas inlets (Table II). In the case of S175, the variation of pressure is obtained by increasing both the nitrogen and silane inlet flow. As expected and in agreement with our previous arguments, we measured a tensile residual stress of +356 MPa.

In the case of sample S177, elaborated at low pumping speed, a longer residence time in the chamber should be expected for all species, allowing them to promote more collisions. The first consequence should be a greater loss of energy for charged species, resulting in an important decrease of ion bombardment, i.e., lowering the compressive stress generation. The measured residual stress is close to zero (+35 MPa); this is the lowest observed stress in this study.

As pointed out by Noskov et al.,[12] stress at the free growing surface of the film is close to zero. Chemical reactions occurring at the surface itself will not result in additional stress in the film. Whereas reactions occurring at the subsurface can promote relaxation phenomena and generate stress. Reactions involving loss of hydrogen could favor the appearance of tensile stress in the films. In many respects, the loss of hydrogen and the related stress are correlated through a complex balance, involving the amount of hydrogen in the films, the ratio between Si–H and Si–NH bonds, the deposition rate, the ion bombardment and the substrate temperature. Our results do not allow to conclude fully on this balance.

Nevertheless, the following hypothesis can be drawn from the above observations: the deposition mechanism should be the result of a competition between, on the one hand, a physical process controlled by ion bombardment and, on the other hand, a chemical process controlled by chemical reactions taking place during deposition. The former is known to favor the generation of a compressive stress in the deposited film.[6–9] For the later, tensile stress[27,28] is mainly generated.

These two opposite behaviors have been pointed out recently by Yota[49] in a comparative study of the properties of silicon nitride films deposited by three different plasma techniques: inductively-coupled plasma high-density plasma chemical vapor deposition (HDP CVD), plasma enhanced chemical vapor deposition (PECVD), and low pressure chemical vapor deposition (LPCVD). The authors show that

TABLE V. Plasma parameters as calculated from Langmuir probe measurements (in Ph.D. thesis M. Lapeyrade- Lyon ECL, 1999). V po =potential at source exit aperture; ΔVp =potential difference between source exit aperture and sample location; Vf = floating potential at sample location; $Vp - Vf$ = Difference between plasma potential and floating potential at sample location; and (22 cm).

Pressure (mTorr)	Vpo(V)	ΔVp (V)	$V_p - V_f$	Ion energy (eV)	Electron temperature (eV)
0.6	40	18	14	32	6.5
1.2	25	16.2	8	24	3
2.3	15	12.8	3.5	16	2.5

the two former films exhibit moderate compressive stress, −1500 and −3800 MPa, respectively, whereas the latter is highly tensile in the GPa range.

The stress variation shown in Fig. 2 can therefore be explained as follows: in the low pressure range, below 1 mTorr, the ion bombardment is strong and controlled the deposition, leading to a highly compressive stress generation; whereas in the high pressure range, above 1.7 mTorr, the ion bombardment is limited and grain growth can thus occur to a large extent. The density of SiN$_x$ films deposited at high pressure is low (Table I), and has been confirmed by the high etch rates obtained for samples S164, S175, S176, and S177. Table I shows the good correlation between etch rate, hydrogen concentration and density of the films: denser films exhibit a low hydrogen content, going along with a low etch rate.

As a last issue in this discussion, we can consider the correlation between the absolute value of the stress and the grain size, i.e., the height and width values. We highlight the relation of internal residual stress to grain size and etch rate. Lower etch rate and grain size are obtained for films deposited at 200 or 300 °C, for a pressure of 1.2 mTorr, 80 and 10 Å min^{-1} respectively, compared to 4 Å min^{-1} for a standard LPCVD Si$_3$N$_4$.

It is noticeable that high stress intensity of −1990 MPa is associated with low grain size (0.8 and 20 nm, respectively, for height and width) and low roughness (rms of 0.2 nm), whereas low stress amplitude of +/−500 MPa is associated with the same rms of 1.5 nm, both for compressive or tensile stress. The difference between the two is a larger grain size (height and width) for tensely strained films than for compressively strained ones: 4.7 and 60 nm for the former and 1 and 40 nm for the latter. This increase of the grain size, in the high pressure range, appears to support a deposition mechanism governed mostly by chemical reactions than ion bombardment, which leads to a grain size increase, going along with the appearance of tensile strain in the films.

Obviously, a complete understanding of the deposition mechanism and aging studies would be needed to fully further understand the phenomena really involved in Si$_3$N$_4$ films deposited by ECR plasma with our equipment. A varying valve pressure would allow the completion of the study of the pressure effect. *In situ* optical measurement of the internal stress during the film deposition, as described in the literature,[35,50] would be of great interest to have some insight into the appearance of tensile stress.

V. CONCLUSION

In this work, the evolution of residual stress in SiN$_x$ films deposited by ECR plasma has been considered versus some deposition parameters (deposition temperature, total pressure) and film thickness. In standard deposition conditions,[32] silicon nitride films exhibit a compressive residual stress at −500 MPa, as the average value, which is the lowest value reported in the literature for films deposited by the ECR plasma technique. AFM observations have shown a granular morphology, with a grain size strongly correlated to the re-

sidual stress intensity. A transition from a compressively strained film to a tensile strained one has been clearly related to the deposition pressure. This transition, occurring in the 1.2–1.4 mTorr range, is rarely observed in PECVD deposited films and related to the configuration of our equipment. This behavior has been related to the deposition mechanism: at low pressure (below 1.2 mTorr), the deposition is mainly controlled, by ion bombardment, leading to high compressive residual stress. On the other hand, at high pressure (above 1.4 mTorr) the mechanism of SiN$_x$ film formation resulted in the combination of a weaker effect of ion bombardment and coalescence between neighboring islands at the subsurface of the film, which leads first to a lower compressive stress, and second to a weak tensile strain generation.

The same behavior has been observed for all types of films deposited with our equipment, i.e., silicon dioxide and hydrogenated silicon films: residual stresses close to zero are obtained for films deposited in the pressure range 1.2–1.5 mTorr. This versatility has been successfully used for the deposition of Si/SiO$_2$ Bragg mirrors involved in the fabrication of tunable photodetectors[51] based on III–V materials, for the infrared region.

[1]D. G. Park *et al.*, J. Vac. Sci. Technol. B **14**, 2674 (1996).
[2]S. Garcia, I. Martil, G. Gonzalez Diaz, E. Castan, S. Duenas, and M. Fernandez, J. Appl. Phys. **83**, 332 (1998).
[3]S. Sitbon, M. C. Hugon, B. Agius, F. Abel, J. L. Courant, and M. Puech, J. Vac. Sci. Technol. A **13**, 2900 (1995).
[4]S. Matsuo, in *Handbook of Thin Films Deposition Processes and Techniques*, edited by K. K Schuegraf (Noyes, Park Ridge, NJ, 1988), p. 147.
[5]A. Shintani, S. Sugaki, and H. Nakashima, J. Appl. Phys. **51**, 4197 (1980).
[6]A. Fourrier, A. Bosseboeuf, D. Bouchier, and G. Gautherin, Jpn. J. Appl. Phys., Part 1 **30**, 1469 (1991).
[7]H. Takahashi, H. Nagata, H. Kataoka, and H. Takai, J. Mater. Res. **10**, 2736 (1995).
[8]J. E. Klemberg-Sapieha *et al.*, J. Vac. Sci. Technol. A **14**, 2775 (1996).
[9]J. H. Kim and K. W. Chung, J. Appl. Phys. **83**, 5831 (1998).
[10]J. Ashley Taylor, J. Vac. Sci. Technol. A **9**, 2464 (1991).
[11]J. G. E. Gardeniers, H. A. C. Tilmans, and C. C. G. Visser, J. Vac. Sci. Technol. A **14**, 2879 (1996).
[12]A. G. Noskov *et al.*, Thin Solid Films **162**, 129 (1988).
[13]L. Shi *et al.*, J. Vac. Sci. Technol. A **14**, 471 (1996).
[14]P. Temple-Boyer, C. Rossi, E. Saint-Etienne, and E. Scheid, J. Vac. Sci. Technol. A **16**, 2003 (1998).
[15]R. M. Kubacki, IEEE Trans. Compon., Packag. Manuf. Technol., Part A **18**, 471 (1995).
[16]J. Ahn and K. Suzuki, Appl. Phys. Lett. **64**, 3249 (1994).
[17]M. Maeda and K. Ikeda, J. Appl. Phys. **83**, 3865 (1998).
[18]F. Delmotte, M. C. Hugon, B. Agius, and J. L. Courant, J. Vac. Sci. Technol. B **15**, 1919 (1997).
[19]W. J. Dauksher *et al.*, J. Vac. Sci. Technol. B **15**, 2232 (1997).

[20]P. J. French, P. M. Sarro, R. Mallée, E. J. M. Fakkeldij, and R. F. Wolffen-buttel, Sens. Actuators, A **58**, 149 (1997).

[21]M. Stadtmüeller, J. Electrochem. Soc. **139**, 3669 (1992).

[22]S. Habermehl, J. Appl. Phys. **83**, 4672 (1998).

[23]T. M. Klein, T. M. Anderson, A. I. Chowdhury, and G. N. Parsons, J. Vac. Sci. Technol. A **17**, 108 (1999).

[24]R. C. Cammarata, J. Electron. Mater. **26**, 966 (1997).

[25]U. Geyer, U. Von Hülsen, and P. Thiyagarajan, Appl. Phys. Lett. **70**, 1691 (1997).

[26]T. J. Vink, M. A. J. Somers, J. L. C. Daams, and A. G. Dirks, J. Appl. Phys. **70**, 4301 (1991).

[27]S. P. Kim and S. K. Choi, Thin Solid Films **379**, 259 (2000).

[28]J. Yu, J. G. Kim, J. O. Chung, and D. H. Cho, J. Appl. Phys. **88**, 1688 (2000).

[29]B. W. Sheldon, K. H. A. Lau, and A. Rajamani, J. Appl. Phys. **90**, 5097 (2001).

[30]J. H. Jeong, D. Kwon, and Y. J. Baik, J. Appl. Phys. **91**, 6333 (2002).

[31]D. Landheer, K. Rajseh, D. Masson, J. E. Hulse, G. I. Sproule, and T. Quance, J. Vac. Sci. Technol. A **16**, 2931 (1998).

[32]M. Lapeyrade, M. P. Besland, C. Meva'a, A. Sibaï, and G. Hollinger, J. Vac. Sci. Technol. A **17**, 433 (1999).

[33]M. F. Lambrinos, M. P. Besland, A. Gagnaire, P. Louis, S. Callard, and J. Joseph, J. Electrochem. Soc. **144**, 2086 (1997).

[34]S. Callard, A. Gagnaire, M. P. Besland, and J. Joseph, Thin Solid Films **313-314**, 479 (1998).

[35]L. B. Freund, J. A. Floro, and E. Chason, Appl. Phys. Lett. **74**, 1987 (1999).

[36]T. E. Retajczyk, and A. K. Sinha, Thin Solid Films **70**, 241 (1980).

[37]G. Moulard, G. Contoux, G. Motyl, G. Gardet, and M. Courbon, J. Vac. Sci. Technol. A **16**, 736 (1998).

[38]I. Sugimoto and S. Nakano, Appl. Phys. Lett. **62**, 2116 (1993).

[39]R. C. Cammarata, T. M. Trimble, and D. J. Srolovitz, J. Mater. Res. **15**, 2468 (2000).

[40]M. A. Bachlechner et al., Appl. Phys. Lett. **72**, 1969 (1998).

[41]M. Copel, P. R. Varekamp, D. W. Kisker, F. R. McFeely, K. E. Litz, and M. M. Banaszak Holl, Appl. Phys. Lett. **74**, 1830 (1999).

[42]N. Suzuki, T. Yoshikawa, K. Masu, K. Tsubouchi, and N. Mikoshiba, Jpn. J. Appl. Phys., Part 2 **28**, L2316 (1989).

[43]J. A. Theil, S. V. Hattangady, and G. Lucovsky, J. Vac. Sci. Technol. A **10**, 719 (1992).

[44]H. Leplan, B. Geenen, J. Y. Robic, and Y. Pauleau, J. Appl. Phys. **78**, 962 (1995).

[45]Y. Park et al., Appl. Phys. Lett. **75**, 3811 (1999).

[46]J. A. Thornton, J. Tabock, and D. W. Hoffman, Thin Solid Films **64**, 111 (1979).

[47]L. B. Freund and E. Chason, J. Appl. Phys. **89**, 4866 (2001).

[48]S. G. Mayr and K. Samwer, Phys. Rev. Lett. **87**, 036105 (2001).

[49]J. Yota, J. Hander, and A. A. Saleh, J. Vac. Sci. Technol. A **18**, 372 (2000).

[50]Y. Kim and S. H. Choo, Thin Solid Films **394**, 283 (2001).

[51]S. Jourba, M.-P. Besland, M. Gendry, M. Garrigues, J.-L. Leclercq, P. Rojo-Romeo, P. Viktorovitch, S. Cortial, X. Hugon, and C. Pautet, Electron. Lett. **35**, 1272 (1999).